difference between these two systems is that System A has large capacity terms and System B comparatively small capacity terms. This difference explains why the dynamic simulation of System B converges much faster to a periodic state than that of System A. For System A Broyden's method reduces the CPU time with a factor five, whereas for System B it is only slightly faster than the dynamic simulation.

For nonlinear systems we have introduced the Newton-Picard method as an alternative to methods more commonly used in chemical engineering literature. It is found that for the weakly nonlinear System C, Broyden's method is fastest and that the Newton-Picard method needs a CPU time equal to the dynamic simulation. For the more strongly nonlinear System D, Broyden's method is again the fastest but here the Newton-Picard also reduces the CPU time as compared to the dynamic simulation by a factor two. The main drawback of the Newton-Picard method is the lengthy first iteration, which arises from the construction of the Jacobian in order to determine a basis for the slowly converging subspace.

In practice, often the periodic states need to be determined for optimization ends. This requires the computation of periodic states over a region in a multidimensional parameter space, with the aim to find an optimal parameter set. Especially in such a case the efficiency of the various methods to identify periodic states is of considerable importance. Thus, the ultimate test for these methods is to compare their performance in combination with optimization or continuation procedures.

In future work the combination of the various methods for obtaining periodic states with both continuation and optimization procedures will be addressed. The final goal is a generic strategy for the analysis, design and optimization of cyclically operated processes.

REFERENCES

1. O. J. Smith IV, A. W. Westerberg, Acceleration of cyclic steady state convergence for pressure swing adsorption models, Industrial and Engineering Chemistry Research. 31 (1992) 1569–1573.
2. D. T. Croft, M. G. Levan, Periodic states of adsorption cycles–I. Direct determination and stability, Chemical Engineering Science. 49 (1994) 1821–1829.
3. H. M. Kvamsdal, T. Hertzberger, Optimization of PSA systems - studies on cyclic steady state convergence, Computers and Chemical Engineering. 21 (1997) 819–832.
4. K. Lust, D. Roose, A. Spence, A. R. Champneys, An adaptive Newton-Picard algorithm with subspace iteration for computing periodic solutions, SIAM Journal on Scientific Computing. 19 (1998) 1188–1209.
5. H. M. Kvamsdal, Studies on modeling, simulation and optimization of PSA systems, Ph.D. thesis, University of Trondheim (1995).
6. E. S. Kikkinides, V. I. Sikavitsas, R. T. Yang, Natural gas desulfurization by adsorption: Feasibility and multiplicity of cyclic steady states, Industrial and Engineering Chemistry Research. 34 (1995) 255–262.
7. T. L. van Noorden, S. M. Verduyn Lunel, A. Bliek, Acceleration of the determination of periodic states of cyclically operated reactors, submitted to Chemical Engineering Science .

Studies in Surface Science and Catalysis 133
G.F. Froment and K.C. Waugh (Editors)

Dynamics and control of a radial-flow ammonia synthesis reactor

N. S. Schbib, M. N. Pedernera, D. O. Borio

Planta Piloto de Ingeniería Química (UNS-CONICET)
Camino La Carrindanga, Km. 7, 8000 Bahía Blanca, ARGENTINA
e-mail: reschbib@criba.edu.ar

Abstract

The steady- and non steady-state simulation of an industrial ammonia converter is presented. The reactor includes two adiabatic radial-flow catalyst beds in series. An interbed (gas-gas) heat exchanger is used to preheat the feed stream. The steady-state results showed good agreement with plant data. The influence of different disturbances (feed composition and temperature, reactor pressure) on the dynamic evolution of the main variables is analysed. The open-loop and closed-loop operation is compared from the standpoint of the reactor stability.

1. INTRODUCTION

In large-scale plants, ammonia synthesis is frequently carried out in adiabatic multi-bed reactors with either quench gas or interstage cooling. Two basic flow configurations exist: axial and radial-flow reactors. Most of the large-scale ammonia plants use radial-flow reactors because this arrangement enables to handle large catalyst volumes and small particle diameters (high catalyst efficiency) without considerable pressure drops. In industrial converters the feed stream is usually preheated before entering the catalyst beds using the heat of reaction. Recently, the internal heat exchange has been explored to improve the outlet conversion in an adiabatic ammonia reactor (Abashar, 2000). The feedback of heat, which is intrinsic to autothermal processes, is a source of reactor instability (van Heerden, 1953; Pedernera et al., 1997; Morud and Skogestad, 1998; Mancusi et al, 2000). The existence of steady-state multiplicity and its connection with the optimal operating points has been analysed in detail in a previous contribution (Pedernera et al., 1999).

In the present paper, the non-steady state simulation of a large-scale radial-flow ammonia converter is carried out, aiming to study the influence of the operating variables on the dynamic and stability of the reactor. By means of a detailed mathematical model, the time responses of the main variables are obtained and compared for two different conditions: open loop (without feedback control) and closed loop.

2. PROCESS DESCRIPTION

A large-scale ammonia converter consisting of two adiabatic radial-flow catalyst beds with interstage cooling is considered in the present paper (Figure 1). The sense of motion in both catalyst beds is centripetal. The feed stream is preheated in an interbed countercurrent heat

exchanger, using the hot gases leaving the first bed. In the closed loop operation, the inlet temperature of the first bed (T_{01}) is regulated by feedback control, manipulating the valve located on the cold by-pass stream ($\lambda\phi$). The inlet temperature of the second bed (T_{02}) can also be controlled by adjusting the feed temperature (T_f) in a heat exchanger outside the converter (not considered in the present paper).

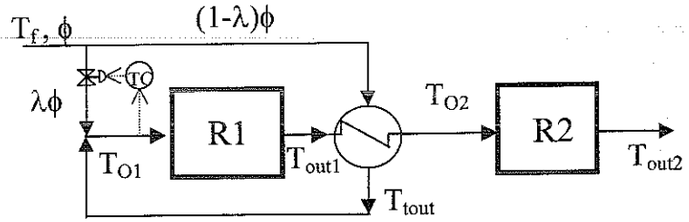

Figure 1: Scheme of the ammonia synthesis reactor

3. MATHEMATICAL MODEL

The catalyst beds are represented by a pseudo-homogeneous one-dimensional model. The converter is assumed to be isobaric. The kinetic expression reported by Temkin (1950) is adopted. The balance equations for the catalyst beds and the heat exchanger are the following:

Catalyst beds

Mass balance:

$$\varepsilon\frac{\partial C_{N_2}}{\partial t} = -\frac{\partial F_{N_2}}{\partial V} - \eta\frac{\alpha R_{NH_3}}{2} \qquad (1)$$

Energy balance:

$$\gamma\frac{\partial T}{\partial t} = -\phi c_{pg}\frac{\partial T}{\partial V} + \eta\alpha R_{NH_3}\left(-\Delta H_r\right) \qquad (2)$$

Heat Exchanger

Energy balance (tube side)

$$\gamma_t\frac{\partial T_t}{\partial t} = -\phi_t c_{pg} L\frac{\partial T_t}{\partial z} + UA(T_{sh} - T_t) \qquad (3)$$

where: $\phi_t = \phi(1-\lambda)$

Energy balance (Shell side)

$$\gamma_{sh}\frac{\partial T_{sh}}{\partial t} = -\phi c_{pg} L\frac{\partial T_{sh}}{\partial z} + UA(T_{sh} - T_t) \qquad (4)$$

Boundary conditions

First bed

$$t = 0 \quad \begin{cases} C_{N_2}(V,0) = C_{N_2}(V)\big|_{ss,1} \\ T(V,0) = T(V)\big|_{ss,1} \end{cases}$$

$$V = 0 \quad \begin{cases} C_{N_2}(0,t) = C_{N_2,f} \\ T(0,t) = T_{01}(t) \end{cases}$$

Second bed

$$t = 0 \quad \begin{cases} C_{N_2}(V,0) = C_{N_2}(V)\big|_{ss,2} \\ T(V,0) = T(V)\big|_{ss,2} \end{cases}$$

$$V = 0 \quad \begin{cases} C_{N_2}(0,t) = C_{N_2}(V_{R1},t) \\ T(0,t) = T_{02}(t) \end{cases}$$

$$t = 0 \quad \begin{cases} C_{N_2}(V,0) = C_{N_2}(V)\big|_{ss,1} \\ T(V,0) = T(V)\big|_{ss,1} \end{cases}$$

$$V = 0 \quad \begin{cases} C_{N_2}(0,t) = C_{N_2,f} \\ T(0,t) = T_{01}(t) \end{cases}$$

where : $T_{01} = \lambda T_f + (1-\lambda)T_{tout}$

Heat exchanger

$$t = 0 \quad \begin{cases} T_t(z,0) = T_t(z)\big|_{ss} \\ T_{sh}(z,0) = T_{sh}(z)\big|_{ss} \end{cases}$$

$$z = 0 \quad \begin{cases} T_t(0,t) = T_f \\ T_{sh}(0,t) = T_{02}(t) \end{cases} \qquad z = L \quad \begin{cases} T_t(L,t) = T_{tout}(t) \\ T_{sh}(L,t) = T_{out1}(t) \end{cases}$$

The efectiveness factor (η) was assumed to be equal to one, based on the small particle diameters used in radial-flow ammonia reactors. This assumption was verified by calculating η through a heterogeneous reactor model (Pedernera et al., 1999). The radial coordinate in the catalyst beds (Eqs. 1, 2) and the axial coordinate in the heat-exchanger (Eqs. 3, 4) are discretized using finite differences, leading to a set of ODE's which are simultaneously integrated along the time using a Gear algorithm. The same set of equations is used to solve the initial steady-state, by setting the time derivative equal to zero in Eqs. 1-4 and solving the resulting algebraic system with a Quasi-Newton method.

4. RESULTS AND DISCUSSION

4.1 Steady state results

The influence of the cold by-pass fraction (λ) on the outlet molar fraction of ammonia is shown in Fig. 2, for different values of the feed temperature (Pedernera et al., 1999). A maximum outlet content of ammonia is obtained at $\lambda \cong 0.417$ for the curve corresponding to $T_f = 230$ °C. This optimal operating point, which is located near the extinction point, has been selected as the reference steady state to obtain the dynamic results shown in item 4.2.

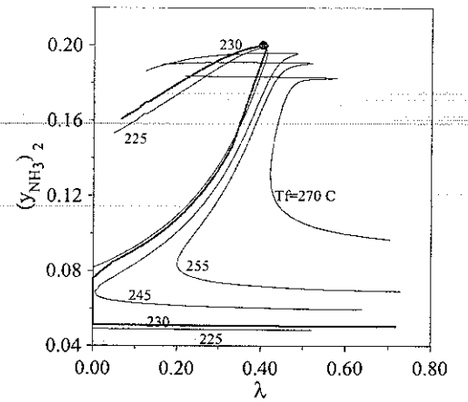

Figure 2: Inlet temperature of the first bed as affected by the cold by-pass, for different T_f.
• Optimal operating point

Figure 3 shows the steady-state radial temperature profiles for the two adiabatic catalytic beds operating at conditions of the optimal point. The corresponding axial temperature profiles in the interbed heat exchanger are also included in Fig. 3, for the tube side (T_t) and shell side (T_{sh}). The simulation results have been compared with industrial data corresponding to a large scale ammonia converter. The deviations at the reactor outlet were less than 0.2% (relative error) in composition and 14 °C in temperature (T_{out2}).

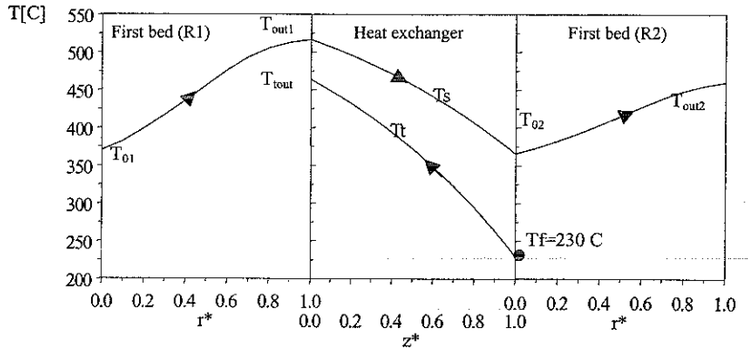

Figure 3: Temperature profiles in the catalyst beds and heat exchanger (T_f = 230 °C ; λ=0.417). $r^* = (r_0 - r)/(r_0 - r_i)$, here r_0, r_i = outer and inner radius of each bed; $z^* = z/L$, where z= axial coordinate and L= tube length in the heat exchanger.

Although a large amount of heat is being transferred in the interbed heat exchanger, the autothermal reactor, when it is considered as a whole, is an adiabatic reactor where a single exothermic reaction is being carried out. Therefore, an almost linear relationship exists between the outlet conversion (x_{N2}) and the overall temperature rise ($\Delta T_{ovl} = T_{out2} - T_f$). As it can be seen in Fig. 4, the variable ΔT_{ovl} is an indirect index of the conversion of N_2 per pass.

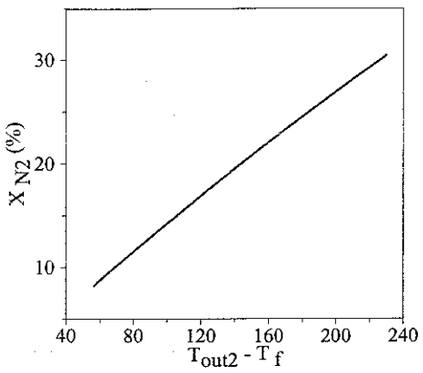

Figure 4: Outlet conversion x_{N2}(%) vs. overall temperature rise ($T_{out2} - T_f$).

4.2 Dynamic results

The time responses of the temperature (deviation variables) at different positions in the reactor are included in Fig. 5, for a positive step change of 10 °C in the feed temperature, T_f (see Fig. 1). An instantaneous change of around 4 °C appears at the inlet of the first bed (T_{01}), due to the sudden increase in the temperature of the cold by-pass (λϕ). The time evolution of T_{01} is a consequence of the heat feedback in the interbed heat exchanger (see the similar shape of the T_{tout} and T_{01} curves). A slight inverse response is observed at the outlet of the first bed (T_{out1}), which is a typical behaviour of fixed bed catalytic reactors. This "wrong way behaviour" influences the temperature at the inlet of the second bed (T_{02}), which oscillates at t≅150 sec.

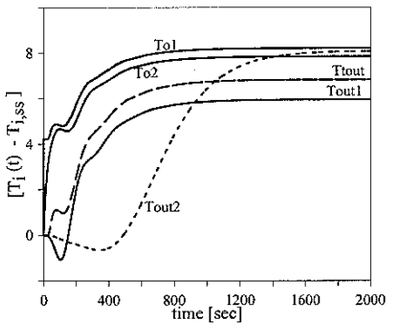

Figure 5: Dynamic evolution of the temperature at different points of the reactor, for a step change ΔT_f=10°C. Deviations from the initial (steady-state) values.

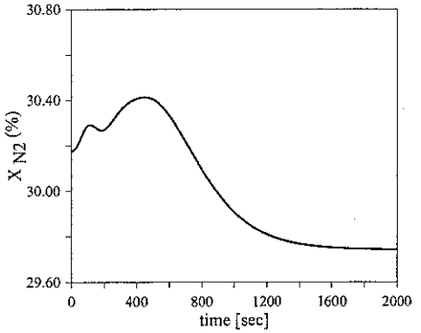

Figure 6: Dynamic evolution of the conversion of N_2 at the reactor outlet, for a step change ΔT_f= 10°C..

The differences between the shape of the T_{out1} and T_{02} curves arise from the dynamics associated to the interbed heat exchanger. An inverse response also appears at the outlet of the second bed (T_{out2}), with a considerable delay with respect to that of the first bed. Fig. 6 shows the transient behaviour of the outlet conversion for the same operating conditions of Fig. 5. As expected, a final drop in conversion appears, because the disturbance in T_f shifts the reactor from its optimal operating conditions. The final conversion drop is in concordance with the results shown in Fig. 5. In fact, for a positive change of 10 °C in T_f, a temperature rise of around 8 °C appears in the variable T_{out2} (final steady state), i.e, ΔT_{ovl} drops around 2 °C when the outlet conversion also decreases from 30.2 to 29.7 %. The transient behaviour of the variable x_{N2} (Fig. 6) is determined by the slow response of the temperature (high heat capacity of the catalyst), which is the source of the overshoot observed in the x_{N2} curve.

The influence of the cold by pass fraction (λ) on the temperature and conversion responses is shown in Figs. 7 and 8. As it was indicated in Fig. 1, λ is one of the manipulated variables when the reactor is operated under feedback control. When a negative step change in λ occurs, the temperature T_{01} shows an instantaneous increase of around 10°C (Fig. 7). This step change in temperature at the inlet of the first bed leads to an initial inverse response in T_{out1} (*wrong way behaviour)*. This inverse response affects the variable T_{tout} in the heat exchanger, and T_{01} is also affected as a consequence of the heat feedback (see Fig. 1). The inlet temperature of the second bed (T_{02}) follows the same initial trend than the T_{out1} curve. However, in contrast to the behaviour observed for T_{out1}, the final value of T_{02} (t=2000 sec.) is lower than the initial one, because of the higher heat transfer rate in the heat exchanger (lower λ implies higher gas flowrate in the tube side). As before, the variable T_{out2} shows an inverse response. Finally, the outlet conversion exhibits a more oscillating response than that observed for the case of a step change in the T_f (compare Figs. 6 and 8).

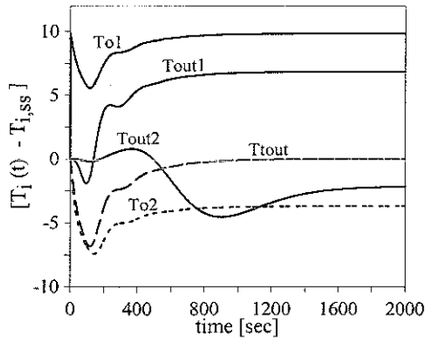

Figure 7: Dynamic evolution of the temperature at different points of the reactor, for a step change in λ from 0.417 to 0.375. Deviations from the initial (steady-state) values.

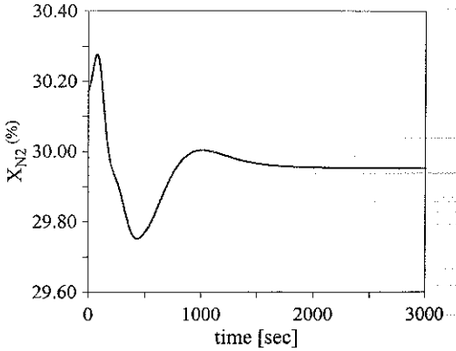

Figure 8: Dynamic evolution of the conversion of N_2 at the reactor outlet, for a step change in λ from 0.417 to 0.375.

The closed loop and open loop reactor dynamics are compared in Figs. 9 and 10, for a step decrease in the reactor pressure. A SISO controller was tuned to control the inlet temperature of the first bed, T_{01}, through the by-pass valve (see Fig. 1). When the reactor is operated without feedback control, the sudden reduction in the pressure leads to a decrease in the heat generation rate, the temperature T_{out1} (and consequently T_{01}) decreases and the reactor moves to a lower (extinguished) steady state. This effect can be seen in Fig. 9, where the overall temperature rise drops from 230 °C to 12 °C. Conversely, when the feedback control loop is included, the overall temperature rise shows a significantly lower decrease (from 230 to 199°C) as a consequence of the gradual reduction of the cold by-pass (Fig. 10).

A similar behaviour is found for the case of an increase in the ammonia contents at the inlet of the converter. In fact, when the molar fraction of ammonia in the feed stream increases, the equilibrium shifts to the reactants and the heat generation rate decreases. If the reactor is being operated under open loop, an extinction phenomenon appears due to the autothermal operation of the converter (Fig. 11). Under closed loop operation, the control action leads to a decrease in the cold by-pass fraction (Fig. 12). As a result, the reactor remains at the upper branch of the curve shown in Fig. 2 (ignited steady-state) and the outlet conversion drops slightly.

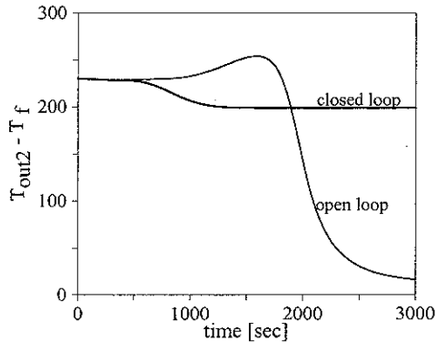

Figure 9: Time responses of the global temperature rise in the converter, after a negative step change in the reactor pressure (ΔP = - 10 atm.).

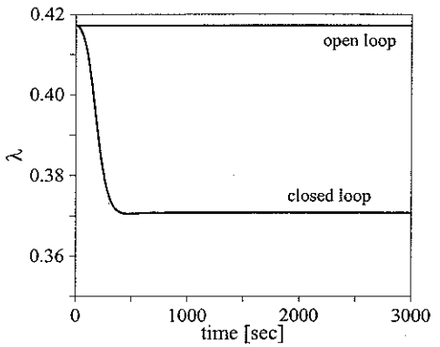

Figure 10: Evolution of the cold by-pass fraction, after a negative step change in the reactor pressure (ΔP = - 10 atm.).

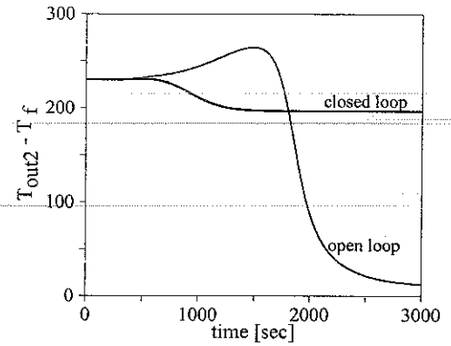

Figure 11: Time responses of the overall temperature rise in the converter, after a positive step change in the amonnia content $(y_{NH3})_f = 0.039 \rightarrow 0.05$

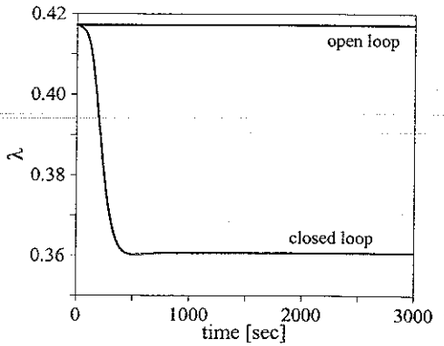

Figure 12: Evolution of the cold by-pass fraction, after a positive step change in the amonnia content , $(y_{NH3})_f = 0.039 \rightarrow 0.05$

5. CONCLUSIONS

By means of a detailed mathematical model, the steady- and non-steady state operation of a large scale ammonia converter have been analysed. The model takes into account the dynamics associated to each catalyst bed and the interbed heat exchanger.

The steady-state results showed good agreement with plant data. The heat feedback associated to the autohermal operation is a source of reactor instability, leading to oscillating time responses and possible extinction of the reaction. This negative effect can be partially compensated by means of a feedback control action, aiming to keep the inlet temperature of the first catalyst bed in the set-point value. In case of changes in the operating conditions of the ammonia synthesis loop, this set-point value (T_{01}) should be adapted to minimise production losses. This procedure could be carried out using an optimisation algorithm that contains the steady-state model of the plant.

NOMENCLATURE

A	heat transfer area, m^2
c_{pg}	mean specific heat of gas, kJ/(kg K)
c_p	specific heat, kJ/(kg K)
C_{N2}	molar concentration of N_2 , $kmol/m^3$
F_{N2}	molar flow of N_2, kmol/s
L	length of the heat exchanger, m
m	mass, kg
P	reactor pressure, atm
r_o, r_i	outer and inter radius of each bed, m
R_{NH_3}	intrinsic reaction rate, $kmol_{NH_3}/(m^3\ s)$

$\gamma = c_{pcat}\,\rho_\beta$

$\gamma_\tau = c_{pg}\,m_{g,t} + c_{pst}m_{st,t}$

$\gamma_{\sigma\eta} = c_{pg}\,m_{g,sh} + c_{pst}m_{st,sh}$

ε	bed porosity, m^3/m^3
ΔH_r	heat of reaction, kJ/ $kmol_{NH_3}$
λ	cold by pass (fraction of ϕ)
η	effectiveness factor
ρ_β	bulk density, kg_{cat}/m^3.

Subscripts

T	temperature, K
t	time,s
U	overall heat transfer coefficient, $kW/(m^2\,K)$
V	reactor volume, m^3
y	molar fraction
z	axial coordinate (heat exchanger), m

cat	catalyst
f	feed
g	gas
sh	shell side (heat exchanger)
ss	steady state
st	steal
t	tube side (heat exchanger).

Greek letters

α	catalyst activity coefficient
ϕ	total mass flow rate, kg/s

REFERENCES

Abashar M. E. E., *Chem. Eng. J.*, 78 (2000), 69-79.

Mancusi E., Merola G., Crescitelli S. and Maffetone P.L., AIChE J. 46 (2000), 824-828.

Morud J. C., Skogestad S., *AIChE Journal*, 44 (1998), 888-895.

Pedernera M. N., Borio D.O., Porras J. A. *AIChE Journal* 43 (1997), 127-134

Pedernera M. N., Borio D. O., Schbib N. S., *Comp. & Chem. Eng.* (1999) S783-S786.

Temkin M., J. Phys. Chem. (USSR) 24 (1950), 1312.

Van Heerden C., *Ind. Eng. Chem.*, 45 (1953), 1242-1247.